Joint International Topical Meeting on Mathematics & Computation and Supercomputing in Nuclear Applications (M&C + SNA 2007)
Monterey, California, April 15-19, 2007, on CD-ROM, American Nuclear Society, LaGrange Park, IL (2007)

VERIFICATION OF THE COUPLED SPACE-ANGLE ADAPTIVITY ALGORITHM FOR THE FINITE ELEMENT-SPHERICAL HARMONICS METHOD VIA THE METHOD OF MANUFACTURED SOLUTIONS

HyeongKae Park and Cassiano R. E. de Oliveira
Nuclear and Radiological Engineering Program,
George W. Woodruff School of Mechanical Engineering,
Georgia Institute of Technology, Atlanta, GA 30332-0405 USA
gtg495p@mail.gatech.edu, c.oliveira@gatech.edu

ABSTRACT

This paper describes the verification of the recently developed space-angle self-adaptive algorithm for the finite element-spherical harmonics method via the Method of Manufactured Solutions. This method provides a simple, yet robust way for verifying the theoretical properties of the adaptive algorithm and interfaces very well with the underlying second-order, even-parity trasnport formulation. Simple analytic solutions in both spatial and angular variables are manufactured to assess the theoretical performance of the *a posteriori* error estimates. The numerical results confirm reliability of the developed space-angle error indicators.

Key Words: Method of Manufactured Solutions, Adaptivity, Finite Elements, Spherical Harmonics

1. INTRODUCTION

Efficient use of computational resources is the key to practical radiation modeling and this has become the main focus of recent research into numerical transport methods. *A posteriori* error analysis combined with adaptive mesh refinement [1] provides a powerful numerical framework for minimizing discretization error and computational effort, and is gradually being recognized as the main way forward. However, though proper implementation of this combined adaptive methodology can potentially enhance the capability of existing computer codes, rigorous verification of the numerical implementation of the theory is necessary in order to avoid the potential performance gains being offset by the added algorithmic complexity.

Verification of deterministic radiation transport methods is traditionally performed by benchmarking the numerical results against Monte Carlo solutions (i.e. [2]). Due to the nature of the Monte Carlo method, the benchmark values are often reported in terms of local integral quantities such as pin power and dose rate, or global characteristics such as the effective multiplication constant (k_{eff}). This kind of benchmarking effort often suffices to check the capability and accuracy of the computer code. However, it does not render itself to assessing the theoretical performance of new algorithms, in particular adaptive ones, since it lacks the fine details of the phase-space solution. An alternative would be to use analytical benchmarks but their range of applicability is somewhat limited.

In this work, we employ the Method of Manufactured Solutions (MMS) [4] to assess the combined space-angle adaptivity algorithm which has been recently developed [3]. The MMS is a simple, yet robust methodology suitable for the analysis of the theoretical properties of numerical schemes. The basic strategy of the MMS is to compute the artificial source term by substituting any desired form of the analytic solutions into the governing differential equations. Thus, a large group of the analytical solutions can be

considered for the numerical tests. In our case, the global analytical solutions are used to evaluate the reliability of the *a posteriori* error indicators rather than comparing the convergence rates.

2. THE METHOD OF MANUFACTURED SOLUTIONS IN THE EVEN-PARITY TRANSPORT FRAMEWORK

2.1. Coupled Space-Angle Adaptivity Algorithm in the Finite Element-Spherical Harmonics Method

Our radiation transport model is based on the variational formulation for the second-order, even-parity form of the transport equation [5] :

$$K^{+}[\psi] = (\mathbf{\Omega}\cdot\nabla\psi, G\mathbf{\Omega}\cdot\nabla\psi) + (\psi, C\psi) + < \psi,\psi > -2(\psi, S^{+}) - 2 < \psi, T > -2(\mathbf{\Omega}\cdot\nabla\psi, GS^{-}) \quad (1)$$

where ψ is the trial function, $S^{\pm}$ are the parity components of the prescribed source, and *G* and *C* are the integral collision operators. Discretization of Eq. (1) is achieved via the well-known Ritz Galerkin method using a trial function of the form:

$$\psi(\mathbf{r},\mathbf{\Omega}) = \sum_{e=1}^{E} B^{eT}(\mathbf{r}) \otimes Q^{T}(\mathbf{\Omega})\psi^{e} \quad (2)$$

where, $B^{e}(\mathbf{r})$ and $Q(\mathbf{\Omega})$ are the vectors that contain the spatial and angular basis function, respectively. Substituting the Eq. (2) into (1) yields the reduced functional:

$$K^{+}[\psi] = \sum_{e=1}^{E} \psi^{eT} A^{e} \psi^{e} - 2\psi^{T} b \quad (3)$$

where,

$$A^{e} = (\mathbf{\Omega}\cdot\nabla B^{eT}\otimes Q^{T}, G\mathbf{\Omega}\cdot\nabla B^{eT}\otimes Q^{T}) + (B^{eT}\otimes Q^{T}, CB^{eT}\otimes Q^{T}) + < B^{eT}\otimes Q^{T}, B^{eT}\otimes Q^{T} > \quad (4)$$

and

$$b^{e} = (B^{eT}\otimes Q^{T}, S^{+}) + < B^{eT}\otimes Q^{T}, T > + (\mathbf{\Omega}\cdot\nabla B^{eT}\otimes Q^{T}, G\mathbf{\Omega}\cdot\nabla S^{-}) \quad (5)$$

Taking the first variation of Eq. (3) and requiring to vanish, we obtain the system of the equation of the form [6]:

$$\mathbf{A}\psi = \mathbf{b} \quad (6)$$

Our adaptivity algorithm employs a residual-based *a posteriori* error analysis [1] and makes use of the hierarchical property of the spherical harmonics basis functions. The spatial convergence of given P_N approximations is first checked against the spatially continuous P_N solution. Then the converged P_N approximation is projected onto the higher-order space in order to estimate the angular truncation errors. We employ the explicit error estimator in the space (Eq. (7)), and the implicit estimator in angular variables (Eq. (8)).

$$\eta_{E}^{2} = \min\{h_{E}^{4}\sigma_{t}^{2}, \frac{1}{\sigma_{a}^{2}}\}||R(\psi_{h,N})||_{L_2(E\times\mathbf{\Omega})}^{2} + \min\{h_{E}^{3}\sigma_{t}^{2}, \frac{1}{\sigma_{a}^{2}}\}||R_{\gamma}(\psi_{h,N})||_{L_2(\partial E\times\mathbf{\Omega})}^{2} \quad (7)$$

$$\begin{aligned} F[\phi, e_{h,N}] &= F[\phi,\psi] - F[\phi,\psi_{h,N}] \\ &= F_{s}[\phi] - F[\phi,\psi_{h,N}] \\ &= \int_{4\pi} d\Omega \int_{V} dV \phi R(\psi_{h,N}) + \int_{4\pi} d\Omega \int_{\partial V} d\Gamma(\mathbf{n}\cdot\mathbf{\Omega})\phi < G(\mathbf{\Omega}\cdot\nabla\psi_{h,N} - S^{-}) > \end{aligned} \quad (8)$$

where η_E is the estimated spatial L_2 discretization error in the element *E*, and functions *R* and R_γ are the finite element residual in the volume and surface term, respectively. The term $e_{h,N}$ is the angular truncation error of the P_N approximation.

2.2. The Method of Manufactured Solutions

As mentioned earlier, the main idea behind the MMS is to compute the artificial source term which results from substituting any desired form for the analytic solutions into the governing differential equations. Due to the implicit treatment of the scattering kernels [6], and separation of the source into the parity components, the MMS framework naturally fits into the even-parity transport formulation. The second-order, even-parity transport equation can be written as:

$$-\mathbf{\Omega}\cdot\nabla G\mathbf{\Omega}\cdot\nabla\phi^{+}+C\phi^{+}=S^{+}-\mathbf{\Omega}\cdot\nabla GS^{-} \tag{9}$$

By simply comparing the RHS and LHS term by term, the parity components of the source terms may be computed from the even-parity flux as:

$$S^{+} = C\phi^{+} \tag{10}$$

$$S^{-} = \mathbf{\Omega}\cdot\nabla\phi^{+} \tag{11}$$

The next step is to specify boundary conditions. Two commonly used boundary conditions are the reflective and the vacuum boundary conditions. The reflective boundary condition can be specified anywhere at the plane of symmetry. On the other hand, the vacuum boundary condition can be used in any location by specifying a suitable surface source. Denoting the even-parity flux at boundary Γ as ϕ_{Γ}, a proper boundary condition can be provided by setting the surface source term *T* to the boundary flux ϕ_{Γ}:

$$T=\phi_{\Gamma} \tag{12}$$

3. NUMERICAL RESULTS

In this section, we present the verification steps of the coupled space-angle adaptivity algorithm by the MMS. The main objective of this verification was to assess the effectiveness of the *a posteriori* error indicators. In order to measure effectiveness of the developed *a posteriori* error estimators, we define the effective index (*EI*) [7] as:

$$EI=\frac{\text{Estimated Error}}{\text{True Error}} \tag{13}$$

It is clear that the error indicator is more effective if the *EI* is closer to one. Moreover, if the *EI* is greater than unity, the adaptivity algorithm is considered as a conservative procedure.

3.1. Measure of Zero Error

The first test case was intended to demonstrate the capability of *a posteriori* error indicator to identify zero error. The problem consisted of a 1.0x1.0cm square region, with total, absorption, and scattering cross section values of 1.0cm^{-1}, 1.0cm^{-1} and 0.0cm^{-1}, respectively. The following form for the solution was considered:

$$\phi^{+}(\mathbf{r},\mathbf{\Omega})=x \tag{14}$$

Since the linear basis function could characterize the solution exactly and there was no angular dependence for this test problem, we expected that no spatial mesh refinement would take place and the computation would terminate at the P_1 approximation. The initial mesh and the resulting flux distribution are shown in Figure 1. The spatial and angular global L_2 errors after the first P_1 calculation were calculated to be 2.305x10^{-8} and 1.929x10^{-8}, respectively, which were within the round-off errors. Both space and angular error estimators were, in fact, computed as effectively zero for this problem.

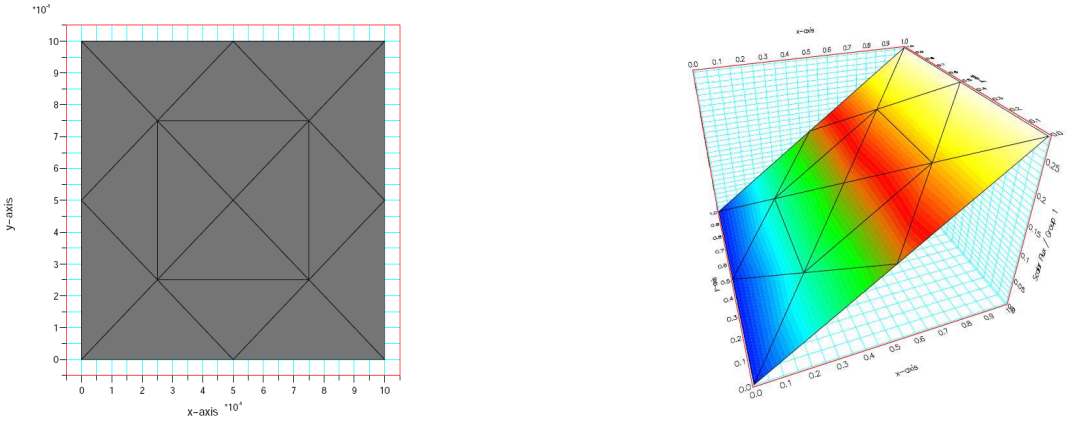

(a) Initial mesh (b) Flux profile

Figure 1. Mesh and Flux Profile of the First Test Problem

3.2. Measure of Non-Zero Discretization Error with Smooth Solution

In the previous section, we have demonstrated that the spatial error indicator successfully estimated zero error. In this section, we assess the validity of the spatial error indicator using simple analytic functions. The test problem consisted of a uniform 10x10cm square region with the total cross section set to $1.0cm^{-1}$, while the absorption and scattering cross sections were left free to vary in order to test the various cross section sets (also see Section 3.2.1). The following even-parity solution was used:

$$\phi^{+}(\mathbf{r},\mathbf{\Omega}) = \sum_{l,even}^{N}\sum_{m=0}^{l}\frac{1}{2^l}(2+\cos[\frac{(l+1)x}{(y+1)}])Y_{l,m}^{e}(\mathbf{\Omega}) \tag{15}$$

The relative convergence criterion was set to 1.0×10^{-4}. Figure 2 shows a relationship between the relative error and total number of nodes in the P_1 approximation. To reach a similar relative error, the adaptive mesh reduced the number of nodes by about a factor of four. From Figure 3, we can observe that, as expected, the adaptive mesh refinement clustered the mesh in the region where a large flux gradient was present.

Table I lists the *EI* for several different spatial resolutions. The effective indices ranged between 3.0 and 4.0 for this test problem, implying that the explicit error indicator provided a conservative estimate. The discrepancy between the exact and estimated error stemed from the unknown constant introduced for the explicit estimators. In the first two iterations, the *EI* was rather large (20.98 and 14.10, respectively). This was due to the inability of the coarse spatial discretizations to model the solution accurately. In such cases, the error indicator did not work properly. This was not necessarily bad because the numerical solutions did not represent the true solution anyway.

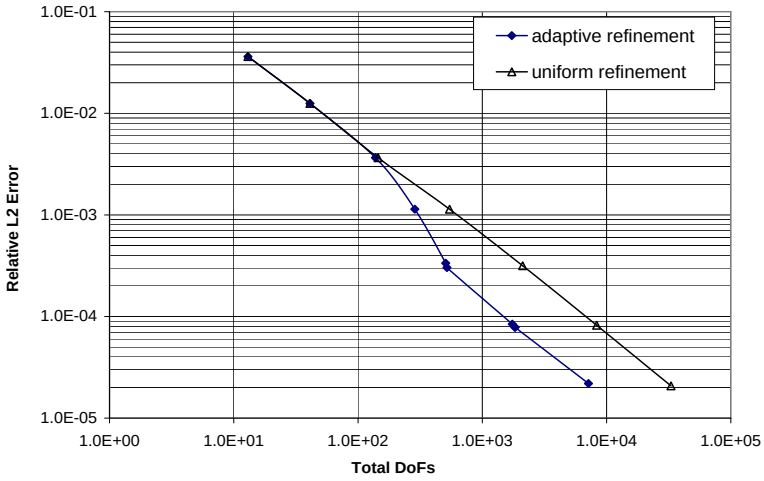

Figure 2. Relative Error v.s. Number of Nodes (Scattering Ratio=0.8)

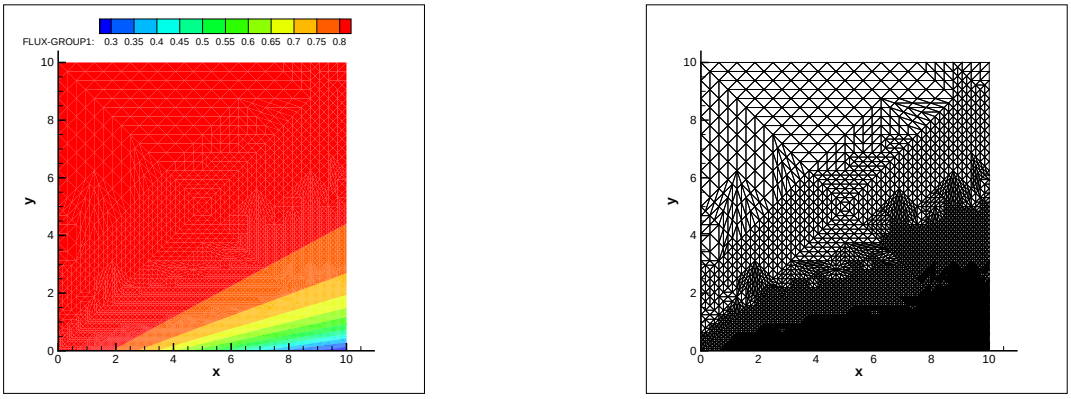

(a) Flux profile (b) Final mesh

Figure 3. Flux Profile and Final Mesh of the Test Problem 2

Table I. Effective Index for Different Spatial Resolutions (Scattering Ratio=0.8)

No. of Nodes	Estimated Error	True Error	Effective Index
13	$7.60\text{x}10^{-01}$	$3.61\text{x}10^{-02}$	21.02
41	$1.35\text{x}10^{-01}$	$1.25\text{x}10^{-02}$	10.76
138	$1.23\text{x}10^{-02}$	$3.66\text{x}10^{-03}$	3.37
286	$3.46\text{x}10^{-03}$	$1.14\text{x}10^{-03}$	3.04
507	$1.16\text{x}10^{-03}$	$3.35\text{x}10^{-04}$	3.45
1743	$3.30\text{x}10^{-04}$	$8.42\text{x}10^{-05}$	3.93
1831	$3.18\text{x}10^{-04}$	$7.83\text{x}10^{-05}$	4.06
7145	$8.49\text{x}10^{-05}$	$2.19\text{x}10^{-05}$	3.87

3.2.1. Effect of cross sections to *a posteriori* error estimate

The next step was to check how the cross sections affected the *a posteriori* error estimates. To this end, the following two sets of problems were solved:

- Varying the magnitude of the total cross section with a fixed scattering ratio
- Varying the scattering ratio with a fixed total cross section

Table II shows the *EI*'s obtained for the different total cross sections, while Table III shows the *EI*'s obtained for the different scattering ratios.

Table II. Effective Index for Various Total Cross Section (Scattering Ratio=0.8)

σ_t	Estimated Error	True Error	Effective Index
0.001	8.55x10^{-05}	3.03x10^{-05}	2.82
0.01	8.28x10^{-05}	2.89x10^{-05}	2.86
0.1	8.34x10^{-05}	2.49x10^{-05}	3.35
1	8.49x10^{-05}	2.19x10^{-05}	3.87
10	5.83x10^{-05}	1.47x10^{-05}	3.96
100	5.91x10^{-05}	3.15x10^{-05}	1.88
1000	5.93x10^{-05}	3.07x10^{-05}	1.93

Table III. Effective Index for for Various Scattering Ratio ($\sigma_t = 1.0\text{cm}^{-1}$)

Scattering Ratio	Estimated Error	True Error	Effective Index
0.001	8.85x10^{-05}	2.05x10^{-05}	4.31
0.01	8.83x10^{-05}	2.05x10^{-05}	4.31
0.1	8.73x10^{-05}	2.04x10^{-05}	4.28
0.8	8.49x10^{-05}	2.19x10^{-05}	3.88
0.9	8.48x10^{-05}	2.26x10^{-05}	3.75
0.99	8.48x10^{-05}	2.44x10^{-05}	3.47
0.999	8.48x10^{-05}	2.49x10^{-05}	3.40
1.000	8.48x10^{-05}	2.50x10^{-05}	3.39

From Table II, we note that the *EI* decreased as the total cross section deviated away from unity. However, in all the cases presented here, the *EI* ranged between 2.0-4.0, which indicated insensitiveness of the *EI* to the cross section magnitudes. The *EI* was much less sensitive to the scattering ratio variations, which can be seen from Table III.

3.2.2. Implicit angular error estimator

The next step was to verify the implicit angular error estimator. The maximum number of angular moments (N) in Eq. (15)was set to 2 and 4, respectively, such that the angularly converged solutions could be obtained by the P_3 and P_5 approximations. Table IV shows the estimated and true angular errors.

From Table IV, it can be seen that the *EI* remained very close to 1.0, a result much better than those for the spatial error indicator. The implicit error estimator solved the local finite element problems and it did not introduce the unknown constant that was introduced in the explicit error estimator. Therefore, as we would have expected, the implicit angular error indicator gave very reliable estimates.

Table IV. Effective Index for Different P_N Order

Maximum P_N=P_3			
P_N	Estimated Error	True Error	Effective Index
$P_1 \rightarrow P_3$	3.12x10^{-00}	3.13x10^{-00}	0.997
$P_3 \rightarrow P_5$	7.22x10^{-05}	1.24x10^{-04}	—
Maximum P_N=P_5			
$P_1 \rightarrow P_3$	3.12x10^{-00}	3.26x10^{-00}	0.957
$P_3 \rightarrow P_5$	9.14x10^{-01}	9.18x10^{-01}	0.996
$P_5 \rightarrow P_7$	6.53x10^{-05}	1.80x10^{-04}	—

3.3. Measure of Non-Zero Discretization Error for a Non-Smooth Solution

In the previous subsection, we verified the adaptivity algorithm for a relatively smooth solution in the uniform region. However, for realistic applications the radiation transport problem often contains large material discontinuities such as the helium-cladding interface in gas-cooled reactors, for example. Since large material discontinuities lead to large flux gradients, spurious oscillations may ocurr in the computed solution. Therefore, the region around the discontinuity must be resolved adequately in order to obtain an accurate solution. In this subsection, we verified the applicability of the developed adaptivity for a system with a large material discontinuity. The system consisted of a 5.0x2.0cm square region with the following manufactured solution:

$$\phi^{+}(\mathbf{r},\mathbf{\Omega}) = \begin{cases} \sigma_{t1}(1-x)+1 & \text{if } x \leq 1.0 \\ e^{-\sigma_{t2}(x-1)} & \text{if } x > 1.0 \end{cases} \tag{16}$$

where $\sigma_{t1,2}$ is the total cross section of the region 1 and 2, respectively. The material discontinuity in this problem occured at $x = 1.0cm$. The relationship between the magnitude of discontinuity and the *EI* is shown in Table V. In this test problem, the effective index ranged between 1.50-2.00 regardless of the magnitude of discontinuity. The expected spurious oscillations were successfully suppressed due to the adaptive refinement around the region of the material discontinuity,

Table V. Effective Index for Non-Smooth, Discontinuous Interface Problem

$\frac{\sigma_{t2}}{\sigma_{t1}}$	Estimated Error	True Error	Effective Index
10	8.03x10^{-05}	4.01x10^{-05}	2.00
100	7.82x10^{-05}	3.97x10^{-05}	1.97
1000	7.78x10^{-05}	5.03x10^{-05}	1.55
10000	7.77x10^{-05}	4.91x10^{-05}	1.58

3.4. A Multigroup Problem

Lastly, we assessed how a multigroup problem affected the *a posteriori* error estimates. We considered a 10x10cm homogeneous, two-group problem with the following manufactured solutions:

$$\phi^{+}(\mathbf{r},\mathbf{\Omega}) = \begin{cases} \sum_{l,even}^{N}\sum_{m=0}^{l}\frac{1}{2^l}(2+\cos[\frac{(l+1)x}{(y+1)}])Y_{l,m}^{e}(\mathbf{\Omega}) & \text{for group 1} \\ \sum_{l,even}^{N}\sum_{m=0}^{l}\frac{1}{2^l}(2+\sin[\frac{(l+1)x}{(y+1)}])Y_{l,m}^{e}(\mathbf{\Omega}) & \text{for group 2} \end{cases} \quad (17)$$

A maximum number of the angular orders (*N*) was set to 4 (i.e. P_5 approximation). Table VI lists the corresponding cross sections for the problem. A relative tolerance of the problem was set to 1.0x10^{-3}.

We first compared how the error reduced as a function of total number of nodes for both uniform and adaptive refinement cases (Figure 4). From Figure 4, we observe that the adaptive mesh case required only about 25% of number of nodes compared to the uniform refinement case. Figure 5 depicts the group 1 and group 2 scalar flux profile and the final mesh produced by the adaptive mesh refinement. The adaptive strategy successfully refined the mesh around the region where large flux gradients occurred.

Table VI. Material Cross Section of the Multigroup Problem

Group 1			
σ_t	σ_a	σ_{s11}	σ_{s12}
1.0	0.5	0.3	0.2
Group 2			
σ_t	σ_a	σ_{s21}	σ_{s22}
1.0	0.5	0.0	0.5

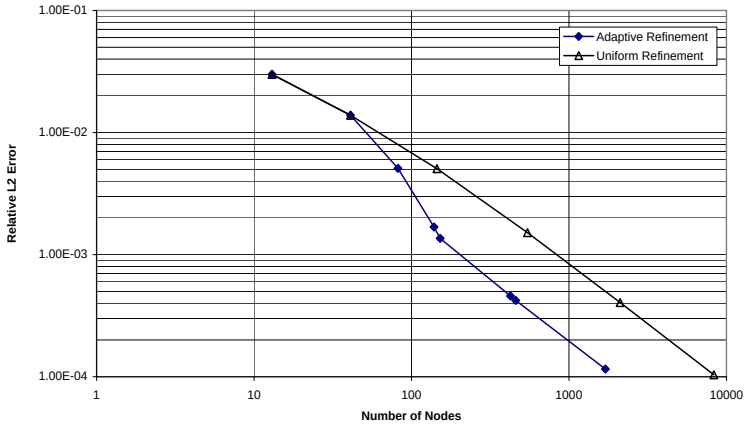

Figure 4. Relative Error v.s. Number of Nodes (Scattering Ratio=0.8)

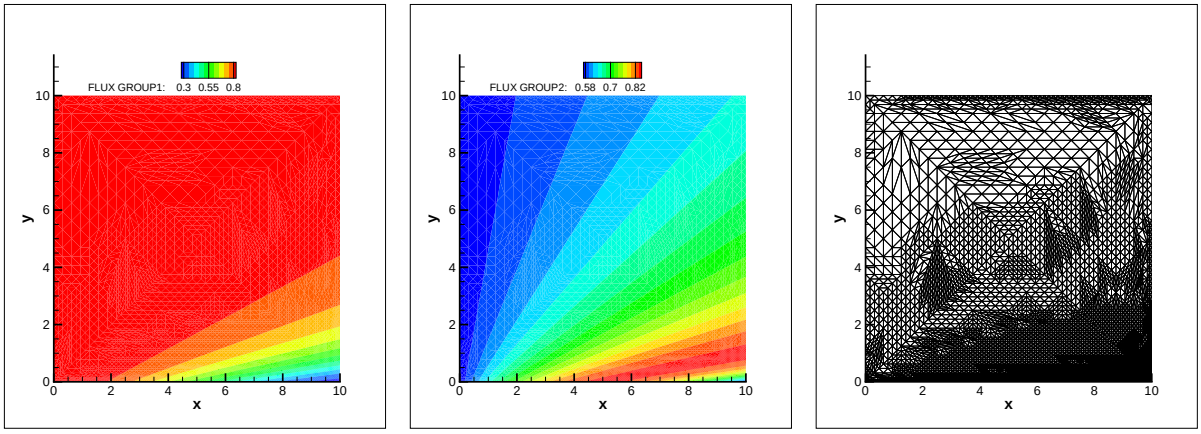

(a) Group 1 (b) Group 2 (c) Final mesh

Figure 5. Flux Profiles and Final Mesh of Multigroup Problem

Table VII shows how the *EI* changed with the number of nodes used in the calculation as well as the *EI* for the angular error estimators. The spatial *EI* was computed by the sum of group 1 and 2 errors, while the angular *EI* was obtained for each group. After the first two spatial iteration steps, the *EI* ranged between 4.25 and 5.27. The *EI* had become quite large compared to the one-group case (i.e. Table I). On the other hand, the difference between true and estimated angular truncation errors was less than 5.0% for all the cases presented.

Table VII. Effective Index for Multigroup Problem

Spatial Error Estimates			
Number of Nodes	Estimated Error	True Error	Effective Index
13	$3.18\text{x}10^{-1}$	$3.00\text{x}10^{-1}$	10.61
41	$1.08\text{x}10^{-1}$	$1.39\text{x}10^{-1}$	7.77
82	$2.69\text{x}10^{-1}$	$5.10\text{x}10^{-1}$	5.27
152	$5.78\text{x}10^{-1}$	$1.36\text{x}10^{-1}$	4.25
459	$2.00\text{x}10^{-1}$	$4.22\text{x}10^{-1}$	4.74
1704	$5.84\text{x}10^{-1}$	$1.16\text{x}10^{-1}$	5.06
Angular Error Estimates Maximum P_N=P_5 (Group1/Group2)			
$P_1 \rightarrow P_3$	$3.12\text{x}10^{-00}$/$3.11\text{x}10^{-00}$	$3.26\text{x}10^{-00}$/$3.26\text{x}10^{-00}$	0.959/0.950
$P_3 \rightarrow P_5$	$9.14\text{x}10^{-01}$/$1.01\text{x}10^{-00}$	$9.18\text{x}10^{-01}$/$1.01\text{x}10^{-00}$	0.997/0.997
$P_5 \rightarrow P_7$	$6.89\text{x}10^{-04}$/$7.03\text{x}10^{-04}$	$1.65\text{x}10^{-03}$/$1.76\text{x}10^{-03}$	—

4. CONCLUSIONS

In this work, the Method of Manufactured Solutions was employed to assess the validity of *a posteriori* error indicators used for coupled space-angle adaptivity based on the second-order, even-parity transport formulation. This formulation provides a natural framework for the application of the MMS as it allows a simple treatment of the source term through the separation into parity components. Several different numerical tests were performed within a unified framework, and the numerical results showed the reliability of the residual-based *a posteriori* error estimators. As a general trend, we have observed that the developed *a posteriori* error indicators closely follow the true error in the angle, while the spatial error indicator somewhat overestimates the true error, and the error indicator is somewhat insensitive to the magnitude of cross section, scattering ratio, and discontinuity.

ACKNOWLEDGMENTS

This work is supported by the US Department of Energy through the Nuclear Engineering Education Research Program (NEER) Award DE-PS07-03ID14540.

REFERENCES

[1] M. Ainsworth and J. T. Oden, "*A posteriori* error estimation in finite element analysis," *Computer Methods in Applied Mechanics and Engineering* **142**, pp. 3771-3796 (1997).

[2] M.A. Smith, E.E. Lewis and B.-C. Na, "Benchmark on deterministic 2-D MOX fuel assembly transport calculations without spatial homogenization," *Progress in Nuclear Energy* **45**, pp. 107-118 (2004).

[3] H. Park and C. R. E. de Oliveira, "Coupled space-angle adaptivity for radiation transport modeling," *Transaction of American Nuclear Society*, Reno, NV. 2006 pp. 514-517.

[4] S. D. Pautz and C. Drumm, "Manufactured solution verification of the ceptre code," *M&C 2005 On Mathematics and Computation, Supercomputing, Reactor Physics and Nuclear and Biological Applications,* Avignon, France, 2005, pp. 234.

[5] R.T. Ackroyd, *Finite element methods for particle transport*, John Wiley and Sons, 1997

[6] C. R. E. de Oliveira, "An arbitrary geometry finite element method for multigroup neutron transport with anisotropic scattering" *Progress in Nuclear Energy*, **18**, pp. 227 (1986).

[7] R. E. Bank, A. Weiser, "Some *a posteriori* error estimators for elliptic partial differential equations," *Mathematics of Computation*, **44**, pp. 281-301, (1985).